Springer

KSME

Journal of Mechanical Science and Technology 32 (10) (2018) 4871~4881
www.springerlink.com/content/1738-494x(Print)/1976-3824(Online)
DOI 10.1007/s12206-018-0935-9

The application of a regularization method to the estimation of geometric errors of a three-axis machine tool using a double ball bar †

Wenjie Tian[1], Guang Yang[1], Lina Wang[2], Fuwen Yin[3] and Weiguo Gao[3,*]

[1]*School of Marine Science and Technology, Tianjin University, Tianjin, China*
[2]*School of Mechanical Engineering, Tianjin Sino-German University of Applied Sciences, Tianjin, China*
[3]*Key Laboratory of Mechanism Theory and Equipment Design of Ministry of Education, Tianjin University, Tianjin, China*

(Manuscript Received February 8, 2018; Revised April 22, 2018; Accepted June 29, 2018)

Abstract

Geometric accuracy is crucially important for machine tools. Identification of geometric errors, especially position-dependent geometric errors, is still a challenging issue. This paper presents a systematic and fast approach to identify the geometric error components of a precision machine tool using double ball bar (DBB). The approach can be implemented in three steps: (1) polynomial based error modeling that relates the DBB radius error directly to the geometric error parameters of machine tool; (2) spatial measurement trajectory planning with a single installation of DBB in order to avoid producing extra setup errors; (3) error identification with regularization method that can solve the ill-posed identification problem effectively. Simulations and experiments show the accuracy and effectiveness of the proposed identification approach. The results of the DBB test show that, utilizing the proposed identification method, the roundness errors of the three circular paths in *xy*-, *yz*- and *xz*-plane are reduced from 27.3 μm, 20.7 μm and 24.1 μm to 9.2 μm, 12.3 μm and 7.8 μm, respectively, with error compensation.

Keywords: Double ball bar; Error identification; Geometric error; Identifiability analysis; Regularization method

1. Introduction

Geometric accuracy is crucially important for machine tools, especially under circumstances where relatively high precision is one of the basic requirements [1-3]. Assuming that sufficient repeatability can be achieved via manufacturing and assembly process, it is well recognized that a practical and economical way for enhancing geometric accuracy is error compensation by software [4], a process by which the actual kinematic parameters can be estimated so as to modify the inverse kinematic model residing in the CNC controller.

The error compensation process falls conventionally into four sequential steps: Modeling, measurement, identification and implementation [5]. In the past, many comprehensive studies and research work have been made in the area of error compensation, and there are two main difficulties: (1) In the measurement process, it is difficult to obtain the geometric error of the machine tool accurately and conveniently; (2) In the identification process, the position-dependent geometric errors [6] are difficult to identify, because each of them changes with axis position and the complicated error model often causes an ill-posed problem [7].

To solve the first problem, many researchers have developed advanced or special measurement devices to detect geometric errors in machines. Basically, all measurement schemes can be classified in two categories: direct and indirect methods. Direct measurements allow the measurement of geometric errors for a single machine axis without the involvement of other axes. Laser-based measurement methods, such as the laser interferometer, are the most common direct methods, which have been widely used for error compensation [8-11]. However, the direct method has the disadvantage that the measurement time is too long to be accepted by industry. Indirect measurements require multi-axes motion of the machine under test. Many studies have been developed based on indirect method with various devices [12-17]. However, the advanced or special device increases the cost of measurement and compensation, especially when the required accuracy is high. In the past decades, double ball bar (DBB), an accurate and economic error measurement system, has been frequently adopted [18-23]. However, current error identification techniques using DBB still have the problems of unsystematic approach, low modeling accuracy due to the small numbers of error components which can be identified, and low order error component models. Therefore, it is necessary to develop a more efficient method in terms of measurement speed and

*Corresponding author. Tel.: +86 2227405280, Fax.: +86 2227405280
E-mail address: gaowg@tju.edu.cn
† Recommended by Associate Editor Byoung-chang Kim

identification accuracy.

As to the second problem, when considering the position-dependent geometric errors, complicated and nonlinear mapping might cause huge difference among all the geometric errors to be identified, which means that some errors influence the tool tip error greatly while others have slight influence. If not all components of volumetric error vector are measured, an ill-posed problem would be even worse because the errors of each axis could not be decoupled. This ill-posed problem even might make identification impossible considering random measurement errors. Usually, optimization of measurement points or adoption of proper algorithm can effectively improve the ill-posed phenomenon. We adopted a regularization method [24-27] to handle this ill-posed problem, instead of choosing optimal measurement points. The solution based on the regularization algorithm is stable and can satisfy the error identification equations so that it will improve the accuracy of identification.

We developed a systematic approach to identify the error components of a machine tool using DBB test. Since circular tests are performed with more than one axis motion involved (usually two), errors measured by a DBB are the combined effects of the error components rather than the errors of single axis. After Sec. 1 has briefly addressed current challenges in error measurement and identification of machine tools, Sec. 2 establishes the volumetric error synthesis model to connect the measured radial errors with all the individual error components of machine. In Sec. 3, identification equations and identifiability analysis are discussed based on the proposed DBB measurement scheme, and a regularization method is also employed to solve the ill-posed identification problem. In Sec. 4, simulation work is realized to certify all the analyses and identification methods mentioned above. Through guidance from simulation, experiments of measurement and identification on a precision horizontal machine tool are presented in Sec. 5. And the results of two verification tests show the effectiveness of the proposed approach. Finally, conclusions are drawn in Sec. 6.

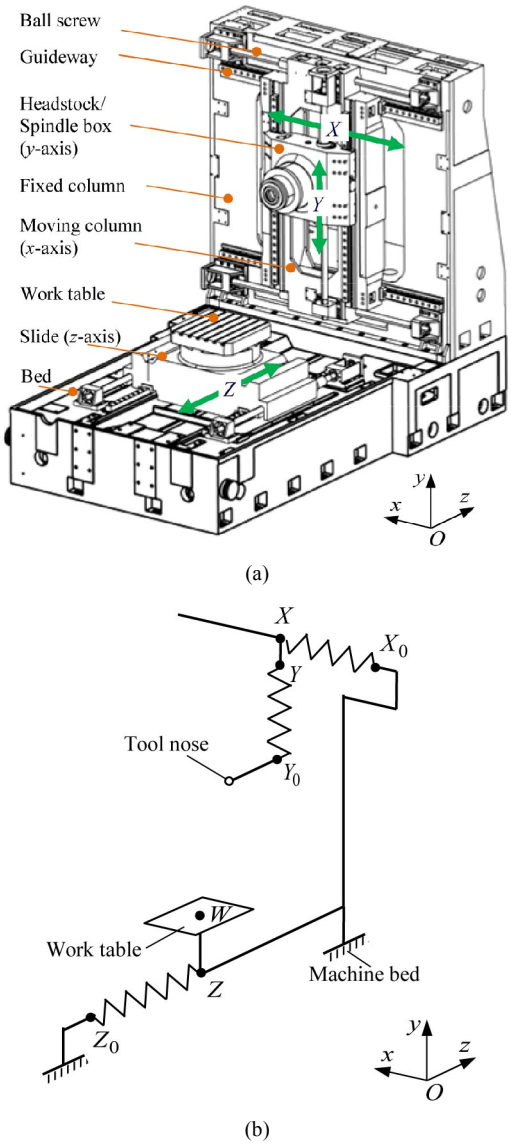

Fig. 1. The experimental 3-axis horizontal machine tool: (a) Structure diagram; (b) kinematic equivalent.

2. System description and error modeling

The experimental 3-axis horizontal machine tool with "box-in-box" construction is shown in Fig. 1. The machine tool is mainly composed of three translational axes: The *x*-axis, which moves the moving column left and right, the *y*-axis, which carries the spindle box up and down, and the *z*-axis, which drives the work table in and out to the spindle.

2.1 Geometric errors of machine tool

The geometric errors of the machine tool refer to the errors of individual axes and those between axes, which are also known as position-dependent geometric errors (PDGEs) and position-independent geometric errors (PIGEs), respectively [6, 28].

PDGEs are the errors of the axis itself and can be modeled as functions of position of this axis. Each axis has six PDGEs, and under the rigid body assumption, the six geometric errors affected by the travel of one axis will not change with positions of the other two axes. Taking *x*-axis as an example (see Fig. 2), reference frame X_0-xyz is located at origin X_0 of *x*-axis, while ideal moving frame $X-xyz$ is fixed on the moving column of *x*-axis and remains parallel to X_0-xyz. The actual position and orientation of frame $X-xyz$ is expressed with frame $X'-xyz$. Due to geometric inaccuracies, there exist six PDGEs, $\delta_x(x)$, $\delta_y(x)$, $\delta_z(x)$, $\varepsilon_x(x)$, $\varepsilon_y(x)$ and $\varepsilon_z(x)$, between frame $X'-xyz$ and $X-xyz$. δ_x, δ_y and δ_z represent the translational errors, where the subscript represents the error direction. ε_x, ε_y and ε_z represent the angular errors, where the subscript represents the rotation axis of angular error. *x*, *y* and *z* are the translational motion coordi-

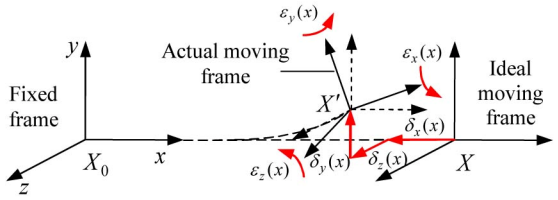

Fig. 2. Linear and angular errors of translational axis (*x*-axis).

nate values of *x*-axis, *y*-axis and *z*-axis, respectively. For example, $\delta_z(x)$ indicates that it is a translational error, an error in *z*-direction, and a function of the *x*-axis position. The PDGEs of *x*-axis can be written in twist form:

$$\boldsymbol{E}(x)=\left(\delta_x(x)\quad \delta_y(x)\quad \delta_z(x)\quad \varepsilon_x(x)\quad \varepsilon_y(x)\quad \varepsilon_z(x)\right)^{\mathrm{T}}.$$

Similarly, the PDGEs of *y*- and *z*-axis can be written as

$$\boldsymbol{E}(y)=\left(\delta_x(y)\quad \delta_y(y)\quad \delta_z(y)\quad \varepsilon_x(y)\quad \varepsilon_y(y)\quad \varepsilon_z(y)\right)^{\mathrm{T}}$$
$$\boldsymbol{E}(z)=\left(\delta_x(z)\quad \delta_y(z)\quad \delta_z(z)\quad \varepsilon_x(z)\quad \varepsilon_y(z)\quad \varepsilon_z(z)\right)^{\mathrm{T}}.$$

PIGEs usually refer to the orientation errors of an axis from its nominal coordinate, and can be regard as constants. Theoretically, one axis has three orientation errors. However, in a real error modeling process, most of them can be neglected due to the reasonable selection of reference coordinate system. For the machine tool shown in Fig. 1, the real motion of *x*-axis is selected as the reference direction; thus *x*-axis has no orientation errors [29]. The plane through *x*-axis and *y*-axis is selected as the reference plane; thus *y*-axis has one orientation error ε_{xy}, namely, the squareness error between *x*-axis and *y*-axis. The nominal direction of *z*-axis is selected such that these three axes construct a right-hand coordinate system; thus the *z*-axis has two squareness errors, ε_{xz} and ε_{yz}. The PIGEs of *x*-, *y*- and *z*-axis can also be written in twist form:

$$\boldsymbol{E}_x=\left(0\quad 0\quad 0\quad 0\quad 0\quad 0\right)^{\mathrm{T}}$$
$$\boldsymbol{E}_y=\left(0\quad 0\quad 0\quad 0\quad 0\quad \varepsilon_{xy}\right)^{\mathrm{T}}$$
$$\boldsymbol{E}_z=\left(0\quad 0\quad 0\quad \varepsilon_{yz}\quad \varepsilon_{xz}\quad 0\right)^{\mathrm{T}}.$$

There are altogether 21 geometric errors for the 3-axis horizontal machine tool: Three translational errors and three angular errors associated with each axis, and one squareness error between every two axes.

2.2 Geometric error model of the DBB-machine system

Fig. 3(a) shows the experimental setup of DBB test on the machine tool. The DBB connects the spindle and the work table with two precision balls and two magnetic sockets. One end of the DBB (P_W) is mounted on the work table, while the

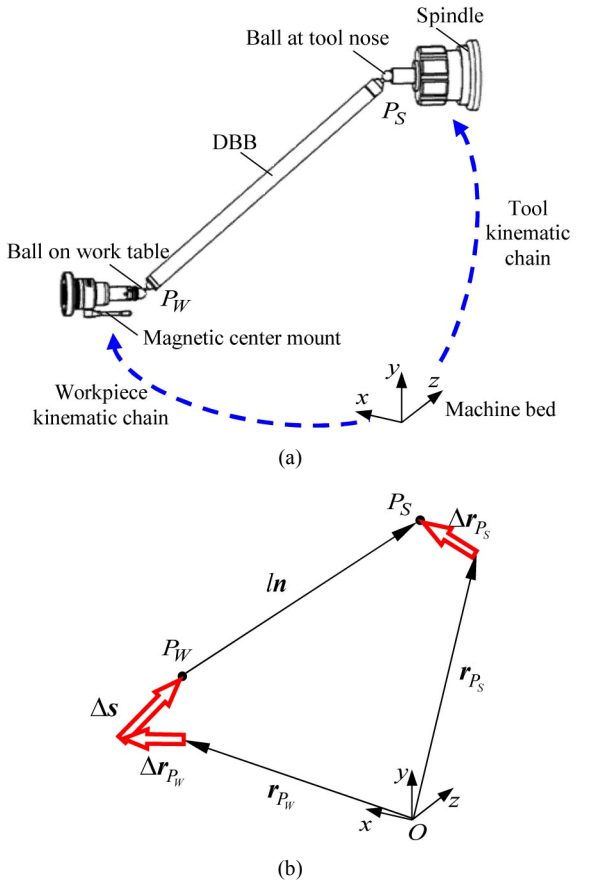

Fig. 3. Measurement setup of DBB-machine system: (a) Structure of DBB instrument; (b) errors of the measurement system.

other (P_S) is attached to the spindle. Inside the DBB there is a relative displacement transducer to detect the extension or contraction of the DBB. The machine is programmed to move along circular paths with a radius equal to the nominal length of the DBB at a certain rate. The radial errors between the actual travel path of the tool and its nominal path are measured and recorded by the DBB.

The volumetric error models of points P_S and P_W need to be established first to connect the measured radial errors with all the individual geometrical errors. From the rigid body kinematics points of view, the spatial displacement error of one point on the rigid body can be considered as resultant of the translational motion error of the reference point and the rotational motion error about the axis passing through the reference point. Therefore, the volumetric error vectors of P_S and P_W, $\Delta\boldsymbol{r}_{P_S}$ and $\Delta\boldsymbol{r}_{P_W}$, can be expressed as

$$\Delta\boldsymbol{r}_{P_S}=\boldsymbol{A}_x\boldsymbol{e}_x+\boldsymbol{A}_y\boldsymbol{e}_y,\quad \Delta\boldsymbol{r}_{P_W}=\boldsymbol{A}_z\boldsymbol{e}_z \tag{1}$$
$$\boldsymbol{e}_x=\begin{pmatrix}\boldsymbol{E}(x)\\ \boldsymbol{E}_x\end{pmatrix},\quad \boldsymbol{e}_y=\begin{pmatrix}\boldsymbol{E}(y)\\ \boldsymbol{E}_y\end{pmatrix},\quad \boldsymbol{e}_z=\begin{pmatrix}\boldsymbol{E}(z)\\ \boldsymbol{E}_z\end{pmatrix}$$
$$\boldsymbol{A}_x=\begin{bmatrix}\boldsymbol{I}_3 & -^{X}\hat{\boldsymbol{r}}_{P_S} & \boldsymbol{I}_3 & -^{X_0}\hat{\boldsymbol{r}}_{P_S}\end{bmatrix}$$
$$\boldsymbol{A}_y=\begin{bmatrix}\boldsymbol{I}_3 & -^{Y}\hat{\boldsymbol{r}}_{P_S} & \boldsymbol{I}_3 & -^{Y_0}\hat{\boldsymbol{r}}_{P_S}\end{bmatrix}$$

$$\boldsymbol{A}_z = \left[\boldsymbol{I}_3 \quad -{}^{Z}\hat{\boldsymbol{r}}_{P_W} \quad \boldsymbol{I}_3 \quad -{}^{Z_0}\hat{\boldsymbol{r}}_{P_W} \right]$$

where $\boldsymbol{e}_x$, $\boldsymbol{e}_y$ and $\boldsymbol{e}_z$ are the error vectors composed of PDGEs and PIGEs of each axis; $\boldsymbol{A}_x$, $\boldsymbol{A}_y$ and $\boldsymbol{A}_z$ are the error mapping matrices; $\boldsymbol{I}_3$ is a unit matrix of order 3, ${}^{j}\boldsymbol{r}_i$ denotes the position vector of point i measured in frame j; $\hat{\boldsymbol{r}}$ is the skew-symmetric matrix of vector $\boldsymbol{r} = (r_x \quad r_y \quad r_z)^{\mathrm{T}}$, and can be expressed as [30]

$$\hat{\boldsymbol{r}} = \begin{bmatrix} 0 & -r_z & r_y \\ r_z & 0 & -r_x \\ -r_y & r_x & 0 \end{bmatrix}.$$

As shown in Fig. 3(b), without consideration of geometric errors, the loop closure equation gives

$$l\boldsymbol{n} = \boldsymbol{r}_{P_S} - \boldsymbol{r}_{P_W} \tag{2}$$

where l and $\boldsymbol{n}$ are the nominal length of the DBB and the nominal unit vector pointing from P_W to P_S. Taking small perturbation on both sides of Eq. (2) yields

$$\Delta l\boldsymbol{n} + l\Delta\boldsymbol{n} = \Delta\boldsymbol{r}_{P_S} - \left(\Delta\boldsymbol{r}_{P_W} + \Delta\boldsymbol{s}\right) \tag{3}$$

where Δl is the DBB radius error; $\Delta\boldsymbol{r}_{P_S}$ and $\Delta\boldsymbol{r}_{P_W}$ are caused by the geometric errors of the machine tool itself and obtained in Eq. (1); $\Delta\boldsymbol{s} = \left(\Delta s_x \quad \Delta s_y \quad \Delta s_z\right)^{\mathrm{T}}$ is induced by the installation error of the magnetic center mount [21]. Note that $\Delta\boldsymbol{s}$ is a constant vector, the elements of $\Delta\boldsymbol{s}$ can be seen as PIGEs. Taking dot products on both sides of Eq. (3) with $\boldsymbol{n}$ and noticing that $\boldsymbol{n}^{\mathrm{T}}\Delta\boldsymbol{n} = 0$ leads to

$$\Delta l = \boldsymbol{n}^{\mathrm{T}}\left(\Delta\boldsymbol{r}_{P_S} - \Delta\boldsymbol{r}_{P_W} - \Delta\boldsymbol{s}\right). \tag{4}$$

Substituting Eq. (1) into Eq. (4), leads to

$$\Delta l = \boldsymbol{h}\boldsymbol{e} \tag{5}$$
$$\boldsymbol{h} = \boldsymbol{n}^{\mathrm{T}}\left[\boldsymbol{A}_x \quad \boldsymbol{A}_y \quad -\boldsymbol{A}_z \quad -\boldsymbol{I}_3\right],\ \boldsymbol{e} = \left(\boldsymbol{e}_x \quad \boldsymbol{e}_y \quad \boldsymbol{e}_z \quad \Delta\boldsymbol{s}\right)^{\mathrm{T}}$$

where $\boldsymbol{e}$ is the geometric error vector of DBB-machine system; $\boldsymbol{h}$ is the corresponding error mapping matrix. Several zero elements in $\boldsymbol{e}$ have no effect on the DBB length error Δl, and should be eliminated, together with the corresponding columns of $\boldsymbol{h}$. At different machine positions, Eq. (5) can relate the DBB radius error directly to the geometric error components.

3. Identification of error parameters with regularization method

As mentioned in Sec. 1, current error identification techniques using DBB still have the problems of unsystematic method and low identification accuracy due to the ill-posed problem. Therefore, it is very necessary to develop a more efficient measurement scheme and a more accurate identification algorithm.

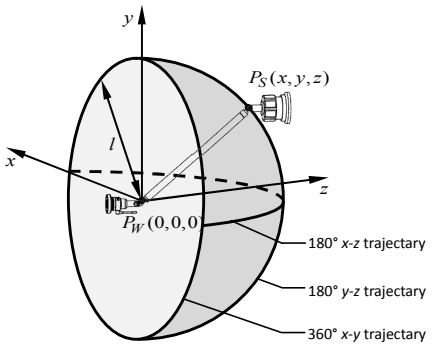

Fig. 4. DBB measurement paths in three coordinate planes.

3.1 DBB measurement scheme

Three circular paths in the *xy*-, *yz*- and *zx*-planes are planned as shown in Fig. 4. The planned measurement paths can be performed with only one mounting of the DBB in order to avoid producing extra setup errors. For the circular path in the *xy*-plane, it is possible to fully trace the circle using DBB. However, tests in the *yz*- and *zx*-plane cannot be performed for full circles due to the interference of the spindle.

At the beginning of the DBB test, the machine tool should be programmed to move the spindle to the center position of the test [31], and the current position of the machine is defined as the origin of the measurement frame $P_W - xyz$, a moving frame fixed on the worktable, by defining a work offset in NC system (see Fig. 4). For convenience, the position coordinate of P_S, (x, y, z), was measured in frame P_W in this study.

3.2 Identification equations

In Sec. 2.2, the radial errors measured by DBB were related to machine volumetric errors by geometric calculations and further related to individual error components by volumetric model. As mentioned above, there are two types of error components in Eq. (5): Position dependent, e.g., $\boldsymbol{E}(x)$, $\boldsymbol{E}(y)$ and $\boldsymbol{E}(z)$, and position independent, e.g., $\boldsymbol{E}_x$, $\boldsymbol{E}_y$, $\boldsymbol{E}_z$ and $\Delta\boldsymbol{s}$. The PDGEs can be described by functions of joint variables. We used the polynomial model to represent each of these error components. For translational PDGEs (positioning errors and straightness errors), we have

$$\delta_i(j) = \sum_{k=0}^{n_1} \delta_{ij,k} \cdot j^k\ ,\quad i, j = x, y, z \tag{6}$$

where n_1 is the order of polynomials and $\delta_{ij,k}$ is the kth coefficient of the polynomial model.

Similarly, for angular PDGEs (pitch, yaw and roll errors),

we have

$$\varepsilon_i(j)=\sum_{k=0}^{n_2}\varepsilon_{ij,k}\cdot j^k\ ,\quad i,j=x,y,z \tag{7}$$

where n_2 is the order of polynomials and $\varepsilon_{ij,k}$ is the kth coefficient of the polynomial model.

Noticing that the DBB test is a kind of relative position measurement method, the geometric errors identified utilizing DBB measurement information are relative errors as well. Let values of PDGEs be zero at the origin P_W, i.e., the constant terms of the error polynomials are set to zero. Thus, Eqs. (6) and (7) can be rewritten in matrix form as

$$\delta_i(j)=\sum_{k=1}^{n_1}\delta_{ij,k}\cdot j^k=\boldsymbol{M}_{\delta_i(j)}\boldsymbol{p}_{\delta_i(j)} \tag{8}$$

$$\boldsymbol{M}_{\delta_i(j)}=\begin{bmatrix}j & j^2 & \cdots & j^{n_1}\end{bmatrix},\ \boldsymbol{p}_{\delta_i(j)}=\begin{pmatrix}\delta_{ij,1} & \delta_{ij,2} & \cdots & \delta_{ij,n_1}\end{pmatrix}^{\mathrm{T}}$$

$$\varepsilon_i(j)=\sum_{k=1}^{n_2}\varepsilon_{ij,k}\cdot j^k=\boldsymbol{M}_{\varepsilon_i(j)}\boldsymbol{p}_{\varepsilon_i(j)} \tag{9}$$

$$\boldsymbol{M}_{\varepsilon_i(j)}=\begin{bmatrix}j & j^2 & \cdots & j^{n_2}\end{bmatrix},\ \boldsymbol{p}_{\varepsilon_i(j)}=\begin{pmatrix}\varepsilon_{ij,1} & \varepsilon_{ij,2} & \cdots & \varepsilon_{ij,n_2}\end{pmatrix}^{\mathrm{T}}$$

where $\boldsymbol{p}_{\delta_i(j)}$ ($\boldsymbol{p}_{\varepsilon_i(j)}$) is the unknown to be identified that contains the parameters of the geometric error $\delta_i(j)$ ($\varepsilon_i(j)$); $\boldsymbol{M}_{\delta_i(j)}$ ($\boldsymbol{M}_{\varepsilon_i(j)}$) is the corresponding mapping matrix.

Taking x-axis as an example, its PDGE vector $\boldsymbol{E}(x)$ can be rewritten using Eqs. (8) and (9) in the following form:

$$\boldsymbol{E}(x)=\underbrace{\begin{bmatrix}\boldsymbol{M}_{\delta_x(x)} & 0_{1\times n_1} & \cdots & 0_{1\times n_2}\\ 0_{1\times n_1} & \boldsymbol{M}_{\delta_y(x)} & \cdots & 0_{1\times n_2}\\ \vdots & \vdots & \ddots & \vdots\\ 0_{1\times n_1} & 0_{1\times n_1} & \cdots & \boldsymbol{M}_{\varepsilon_z(x)}\end{bmatrix}}_{6\times 3(n_1+n_2)}\underbrace{\begin{pmatrix}\boldsymbol{p}_{\delta_x(x)}\\ \boldsymbol{p}_{\delta_y(x)}\\ \vdots\\ \boldsymbol{p}_{\varepsilon_z(x)}\end{pmatrix}}_{3(n_1+n_2)\times 1}. \tag{10}$$

Similarly, the PDGE vectors $\boldsymbol{E}(y)$ and $\boldsymbol{E}(z)$ can be written in the same form. Substituting $\boldsymbol{E}(x)$, $\boldsymbol{E}(y)$ and $\boldsymbol{E}(z)$ into Eq. (5) leads to a vector representation of the DBB length error Δl_i

$$\Delta l_i=\boldsymbol{H}_i\boldsymbol{p} \tag{11}$$

where $\boldsymbol{p}$ is the parameter vector of geometric errors containing $9(n_1+n_2)$ parameters of PDGEs, 3 squareness errors and 3 DBB setup errors; $\boldsymbol{H}_i$ is the mapping matrix with 1 row and $9(n_1+n_2)+6$ columns, the subscript i represents the ith measurement configuration; Δl_i is the DBB length error of the ith measurement configuration. Taking all m measurement configurations into consideration leads to m identification equations.

$$\Delta\boldsymbol{l}=\boldsymbol{H}\boldsymbol{p} \tag{12}$$

$$\Delta\boldsymbol{l}=\begin{pmatrix}\Delta l_1 & \Delta l_2 & \cdots & \Delta l_m\end{pmatrix}^{\mathrm{T}},\ \boldsymbol{H}=\begin{pmatrix}\boldsymbol{H}_1 & \boldsymbol{H}_2 & \cdots & \boldsymbol{H}_m\end{pmatrix}^{\mathrm{T}}.$$

Table 1. The parameters to be identified and their coefficients.

Axis	Geometric errors	Parameters	Coefficients
x-axis	$\delta_x(x)$	$\delta_{xx,1}$	$n_x(ln_x)$
		$\delta_{xx,2}$	$n_x(ln_x)^2$
		⋮	⋮
	$\delta_y(x)$	$\delta_{yx,i}$	$n_y(ln_x)^i$
	$\delta_z(x)$	$\delta_{zx,i}$	$n_z(ln_x)^i$
	$\varepsilon_x(x)$	$\varepsilon_{xx,i}$	$\left(-n_y{}^X z_{P_S}+n_z{}^X y_{P_S}\right)(ln_x)^i$
	$\varepsilon_y(x)$	$\varepsilon_{yx,i}$	$\left(n_x{}^X z_{P_S}-n_z{}^Y x_{P_S}\right)(ln_x)^i$
	$\varepsilon_z(x)$	$\varepsilon_{zx,i}$	$\left(-n_x{}^X y_{P_S}+n_y{}^Y x_{P_S}\right)(ln_x)^i$
y-axis	$\delta_x(y)$	$\delta_{xy,i}$	$n_x(ln_y)^i$
	$\delta_y(y)$	$\delta_{yy,i}$	$n_y(ln_y)^i$
	$\delta_z(y)$	$\delta_{zy,i}$	$n_z(ln_y)^i$
	$\varepsilon_x(y)$	$\varepsilon_{xy,i}$	$\left(-n_y{}^Y z_{P_S}+n_z{}^Y y_{P_S}\right)(ln_y)^i$
	$\varepsilon_y(y)$	$\varepsilon_{yy,i}$	$\left(n_x{}^Y z_{P_S}-n_z{}^Y x_{P_S}\right)(ln_y)^i$
	$\varepsilon_z(y)$	$\varepsilon_{zy,i}$	$\left(-n_x{}^Y y_{P_S}+n_y{}^Y x_{P_S}\right)(ln_y)^i$
z-axis	$\delta_x(z)$	$\delta_{xz,i}$	$-n_x(ln_z)^i$
	$\delta_y(z)$	$\delta_{yz,i}$	$-n_y(ln_z)^i$
	$\delta_z(z)$	$\delta_{zz,i}$	$-n_z(ln_z)^i$
	$\varepsilon_x(z)$	$\varepsilon_{xz,i}$	$\left(n_y{}^W z_{P_W}-n_z{}^Z y_{P_W}\right)(ln_z)^i$
	$\varepsilon_y(z)$	$\varepsilon_{yz,i}$	$\left(-n_x{}^W z_{P_W}+n_z{}^W x_{P_W}\right)(ln_z)^i$
	$\varepsilon_z(z)$	$\varepsilon_{zz,i}$	$\left(n_x{}^Z y_{P_W}-n_y{}^W x_{P_W}\right)(ln_z)^i$
Others	DBB setup errors	Δs_x	$-n_x$
		Δs_y	$-n_y$
		Δs_z	$-n_z$
	Squareness errors	ε_{xy}	$-n_x{}^{Y_0} y_{P_S}+n_y{}^{Y_0} x_{P_S}$
		ε_{yz}	$n_y{}^{Z_0} z_{P_W}-n_z{}^{Z_0} y_{P_W}$
		ε_{xz}	$-n_x{}^{Z_0} z_{P_W}+n_z{}^{Z_0} x_{P_W}$

3.3 Identifiability analysis

To identify the vector $\boldsymbol{p}$ using Eq. (12), special care must be taken to make the columns of matrix $\boldsymbol{H}$ linearly independent. Thus, all the elements of $\boldsymbol{p}$ must be independent. By means of column correlation analysis, there exist two kinds of correlation problems: inevitable linear correlation and potential linear correlation.

Inevitable linear correlation: All of the parameters to be identified and their coefficients are listed in Table 1. It can be

Table 2. Potential linear correlative geometric errors and their prerequisites of linear uncorrelation.

Groups	Geometric errors	Prerequisites of linear uncorrelation
1	$\delta_x(x)$, $\varepsilon_y(x)$, $\varepsilon_z(x)$	${}^{Y}x_{P_S} \neq 0$
2	$\delta_x(y)$, $\varepsilon_y(y)$, $\varepsilon_z(y)$	${}^{Y}x_{P_S} \neq 0$
3	$\delta_y(y)$, $\varepsilon_x(y)$, $\varepsilon_z(y)$	${}^{Y}y_{P_S} \neq 0$
4	$\delta_z(z)$, $\varepsilon_y(z)$, $\varepsilon_z(z)$	${}^{W}x_{P_W} \neq 0$
5	$\delta_z(z)$, $\varepsilon_x(z)$, $\varepsilon_y(z)$	${}^{W}z_{P_W} \neq 0$

seen that the parameter $\delta_{yx,1}$ of $\delta_y(x)$ is linearly dependent on the parameter $\delta_{xy,1}$ of $\delta_x(y)$ under all conditions. It is also true for the parameter $\delta_{zx,1}$ of $\delta_z(x)$ on the parameter $\delta_{xz,1}$ of $\delta_x(z)$ and the parameter $\delta_{zy,1}$ of $\delta_z(y)$ on the parameter $\delta_{yz,1}$ of $\delta_y(z)$. Therefore, $\delta_{yx,1}$, $\delta_{zx,1}$ and $\delta_{zy,1}$ are eliminated, together with the corresponding columns of $\boldsymbol{H}$.

Potential linear correlation: Except the three groups of inevitable linear correlated geometric errors, there also exist five groups of potential linear correlated geometric errors that merit our attention. It can be found in Table 1 that $\delta_x(x)$, $\varepsilon_y(x)$ and $\varepsilon_z(x)$ will be linear correlated when ${}^{Y}x_{P_S} = 0$. It means that the prerequisite for each of them to be identifiable is ${}^{Y}x_{P_S} \neq 0$. Similarly, the other four groups of geometric errors and their prerequisites of linear uncorrelation are together listed in Table 2. To make each geometric error in Table 2 identifiable, the installation position of the DBB must meet two requirements: (1) Ball P_S is not in the spindle axis; (2) ball P_W is not in the longitudinal central axis of the worktable.

After above-mentioned processing, there remain $9(n_1+n_2)+3$ independent parameters in $\boldsymbol{p}$. Therefore if the number of measurement configurations on the planned paths, $m \geq \dim(\boldsymbol{p})$, $\boldsymbol{p}$ is identifiable theoretically.

3.4 Identification algorithm based on regularization method

Although simplified measurement scheme is proposed, it is also very difficult to solve the identification Eq. (12) because of the ill-posed problem.

We employed the Ridge regression method to solve the ill-posed problem, which is a kind of regularization method, and was presented by Hoerl [32] in 1970s. The Ridge regression method tries to substitute a precise solution with an approximate one. The approximate solution is supposed to keep the residual error of the equation low and avoid itself from divergence. With this method, the measurement points can be arbitrarily selected, which will also bring convenience.

The regularization solution of Ridge regression can be expressed as

$$\hat{\boldsymbol{p}} = \left(\boldsymbol{H}^{\mathrm{T}}\boldsymbol{H} + \mu\boldsymbol{I}\right)^{-1}\boldsymbol{H}^{\mathrm{T}}\Delta\boldsymbol{l} \tag{13}$$

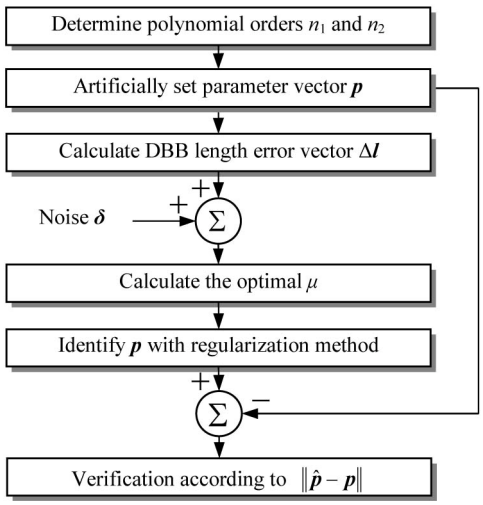

Fig. 5. Simulation procedure of the Regularization method.

where $\hat{\boldsymbol{p}}$ is the identification result of $\boldsymbol{p}$; $\boldsymbol{I}$ is the identity matrix; μ is the regularization parameter (positive and finite).

The value of μ determines how sensitive the solution $\hat{\boldsymbol{p}}$ is to the measurement noise; thus how to obtain the optimal value of μ becomes a key problem. Generalized cross-validation (GCV), due to Wahba [33, 34], is an effective method for practical problems with discrete data and stochastic noise. The GCV parameter estimate is defined by

$$\mu^* = \operatorname{argmin}\left\{\frac{m\left\|\boldsymbol{I} - \boldsymbol{A}(\mu)\Delta\boldsymbol{l}\right\|}{\left[\operatorname{tr}\left(\boldsymbol{I} - \boldsymbol{A}(\mu)\right)\right]^2}\right\} \tag{14}$$

where $\boldsymbol{A}(\mu) = \boldsymbol{H}\left(\boldsymbol{H}^{\mathrm{T}}\boldsymbol{H} + \mu\boldsymbol{I}\right)^{-1}\boldsymbol{H}^{\mathrm{T}}$, m denotes the number of measurement points; tr(•) denotes the trace of the matrix.

4. Simulations

In this section, simulation work is realized to certify the identification method mentioned above. As shown in Fig. 5, the procedure of simulation can be summarized as follows.

Step 1: Determine the orders of the polynomial model, n_1 and n_2;

Step 2: Artificially set parameter vector $\boldsymbol{p}$;

Step 3: Calculate the DBB length error vector $\Delta\boldsymbol{l}$ using Eq. (5), and then artificially add random error vector $\boldsymbol{\delta}$ on $\Delta\boldsymbol{l}$ to simulate the measurement errors;

Step 4: Calculate the optimal μ with GCV method, and identify parameter vector $\boldsymbol{p}$ with Regularization method;

Step 5: Calculate the deviation of $\hat{\boldsymbol{p}}$ from $\boldsymbol{p}$, and verify the effectiveness of the proposed identification method.

To determine appropriate n_1 and n_2, a large amount of actual measurement data with laser interferometer was collected, and the polynomial model with different orders was utilized to fit the normalized error curves. As listed in Table 3, two indices, maximum and root mean square (RMS) of the fitting errors were taken to evaluate the goodness of fit when the fitting

Table 3. Polynomial fitting errors of geometric errors (dimensionless).

Fitting polynomial order	Fitting errors of translational errors (using 68 sets of error data in total)		Fitting errors of angular errors (using 54 sets of error data in total)	
	Max	RMSE	Max	RMSE
1	1.962	1.014	1.709	0.889
2	1.633	0.879	1.566	0.806
3	1.162	0.609	1.219	0.652
4	1.018	0.596	1.107	0.584
5	1.197	0.629	1.008	0.560
6	1.387	0.730	1.298	0.681
7	1.506	0.793	1.417	0.750

Table 4. Identification simulations with regularization method.

Noise (μm)	0.1	0.5	1.0
μ^* (dimensionless)	5.95×10^{-5}	1.20×10^{-4}	9.41×10^{-4}
$\|\hat{\boldsymbol{p}}-\boldsymbol{p}\|$ (dimensionless)	1.74×10^{3}	1.99×10^{3}	2.07×10^{3}
Workspace error (μm)	0.886	1.509	2.317
Contouring error RMS (μm)	0.392	0.820	1.147

polynomial order changes from 1 to 7. With the increased order, the fitting errors of both translational and angular errors reduced at first and then increased due to Runge's phenomenon. Based on an overall consideration of fitting accuracy and model complexity, $n_1 = 3$ and $n_2 = 4$ were selected to establish the polynomial models of Eqs. (8) and (9).

The elements of $\boldsymbol{p}$ were artificially given, and Gaussian noise with standard deviation of 0.1 μm, 0.5 μm and 1.0 μm was added to the measurements (to the DBB readings) to simulate measurement noise. Table 4 gives the simulated identification results. The identification error is calculated as the 2-norm of the difference between the given parameters and the identified parameters. To determine the resulting error improvement, the workspace error after error compensation was simulated using the geometric error model Eq. (1). The workspace error was computed as the average volumetric error at 6^3 equally spaced points in the machine's workspace. And the contouring error after compensation was computed as the root mean square error following along the planned paths shown in Fig. 4. The simulation results verify the effectiveness of the error model and the identification method.

5. Experiment

5.1 Measurement

Fig. 6 shows the horizontal machine tool under investigation and the DBB measurement system, and Fig. 7 shows the detailed measurement paths in three test planes. Angular overshoot, an arc travelled by the tip of the DBB transducer before and after the data capture arc, is programmed to allow the machine to accelerate to the required feed rate before the DBB

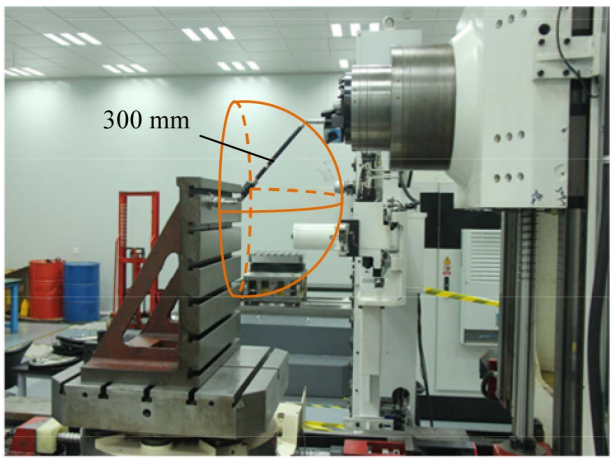

Fig. 6. Horizontal machine tool and DBB measurement system.

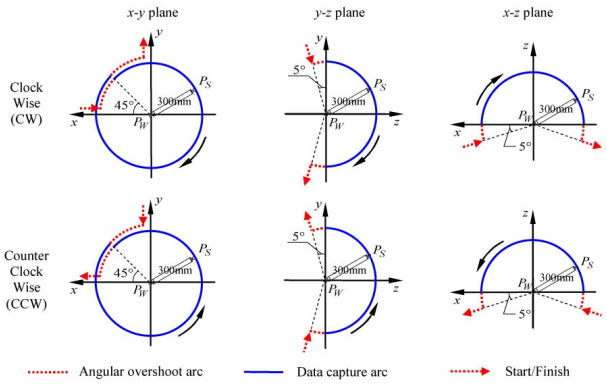

Fig. 7. Angular overshoot arcs and data capture arcs in three DBB test planes.

passes through the data capture arc, and to decelerate before the feed out movement is performed. In this paper, 45°, 5° and 5° overshoots were used in *xy*-, *yz*- and *xz*-plane, respectively.

To reduce the influences of servo-following errors and servo mismatch on DBB measurement data, the experiment was performed with a relatively low feed rate of 600 mm/min. The machine tool was warmed up by preliminary movement for approximately 2 hours prior to the experiment. The thermostatic room temperature was kept between 20.2 ºC and 20.8 ºC during the experiment, and the DBB was kept in the experiment room prior to the experiment to ensure thermal stability. The DBB was calibrated using the Zerodur calibrator provided by the supplier. The numerical resolution of DBB is 0.1 μm.

5.2 Error identification

Each measurement path was conducted five times with a single setup. The averaged measurement data $\Delta \boldsymbol{l}$ is shown in Fig. 8, which was used to identify the parameters in $\boldsymbol{p}$. And then GCV method was used to obtain the regularization parameter. As shown in Fig. 9, the optimal regularization parameter is lo-

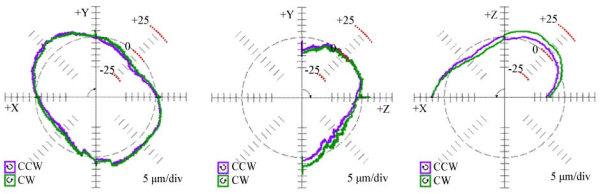

(a) *x*-*y* plane (b) *y*-*z* plane (c) *x*-*z* plane

Fig. 8. Measured and averaged data with five repetitions in three test planes (1 division = 5 μm).

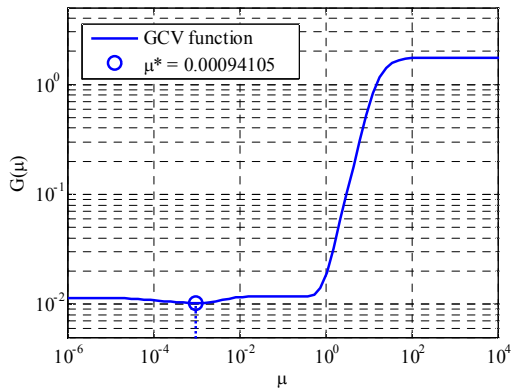

Fig. 9. Optimal regularization parameter selection with GCV method (minimum at $\mu = 9.4105\times10^{-4}$).

cated at the minimum of the GCV curve, and the optimal solution $\mu^* = 9.4105\times10^{-4}$. Substituting μ^* into Eq. (13), all of the parameters in $\boldsymbol{p}$ can be identified. Finally, the estimated PDGEs can be derived using Eqs. (8) and (9). The estimated PDGEs of *x*-, *y*- and *z*-axis are shown in Figs. 10(a)-(c), respectively. In addition, three squareness errors ε_{xy}, ε_{yz} and ε_{xz} and the DBB installation error $\Delta\boldsymbol{s}$ can be directly obtained from the identified $\hat{\boldsymbol{p}}$: $\varepsilon_{xy} = -25.1$ μm/m, $\varepsilon_{yz} = -11.8$ μm/m, $\varepsilon_{xz} = 10.3$ μm/m, $\Delta\boldsymbol{s} = (0.009 \;\; 0.016 \;\; -0.003)^{\mathrm{T}}$ mm.

5.3 Experimental verification

To evaluate the accuracy of the identification method, two experiments were designed and performed as follows.

5.3.1 Experiment 1 (before error compensation)

The procedure of Experiment 1 is shown as follows.

Step 1: Select 25 verification points along a hemispherical helix of center (0, 0, 0) and radius 300 mm (see Fig. 11);

Step 2: Predict the DBB length error $\Delta l_{i,predicted}$ ($i = 1,2,\cdots,25$) using the identified geometric errors;

Step 3: Measure the real DBB length error $\Delta l_{i,measured}$ ($i = 1,2,\cdots,25$) for 5 times;

Step 4: Compare the predicted errors and the measured errors.

Fig. 12 shows the experiment results. Red dashed line denotes the predicted DBB length errors, blue squares denote the mean values of the measured errors, and half the length of the error bar denotes the expanded measurement uncertainty. The

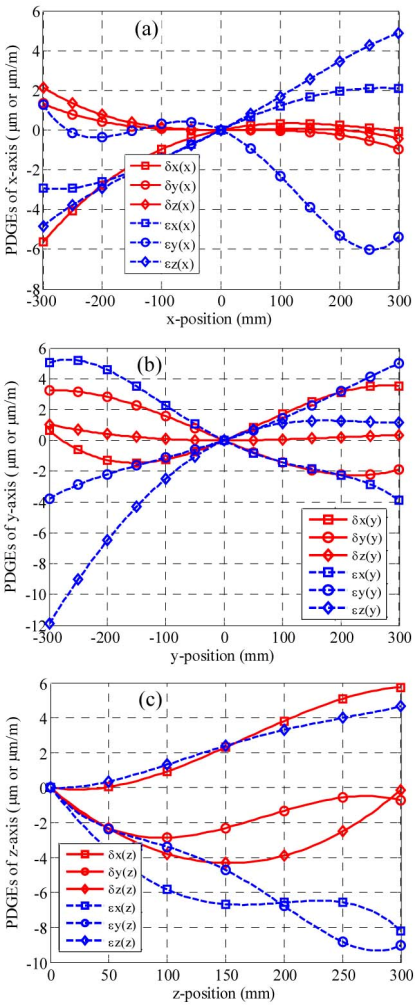

Fig. 10. Identification results of PDGEs of *x*-, *y*- and *z*-axis (unit: μm for translational errors and μm/m for angular errors).

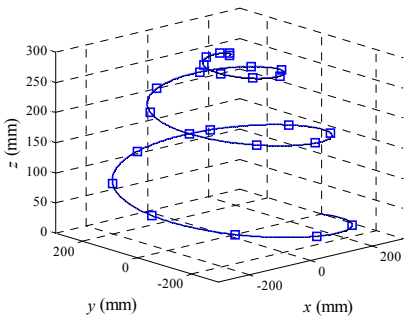

Fig. 11. Verification points along the hemispherical helix.

maximum deviation between the measured and predicted length error is 2.8 μm, which testifies to the high accuracy of the proposed identification method.

5.3.2 Experiment 2 (after error compensation)

Substituting all the identified geometric errors into the error model, we can predict the volumetric errors of the tool relative

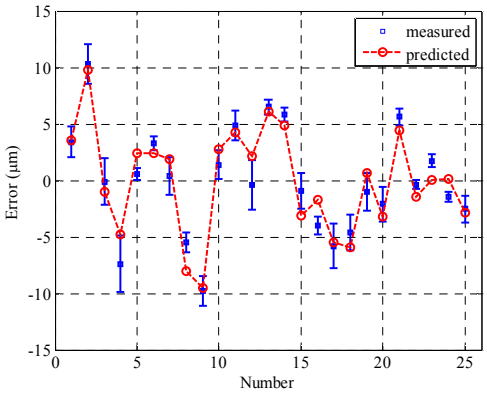

Fig. 12. The discrepancy between the predicted and measured length errors of the DBB.

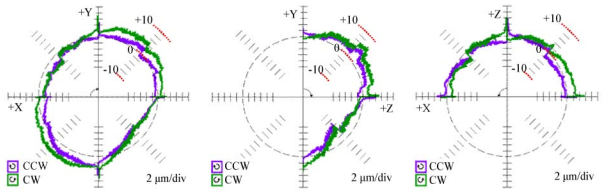

(a) *x*-*y* plane (b) *y*-*z* plane (c) *x*-*z* plane

Fig. 13. DBB test data with error compensation in three planes (1 division = 2 μm).

to the workpiece at any point in the 600×600×300 mm^3 workspace. Then the 3D error compensation was carried out with FANUC 31i NC system. Finally, the DBB test with the same paths and running parameters (see Fig. 6) was performed again to evaluate the special geometric accuracy of the machine tool. The results of the circular test are shown in Fig. 13. Compared with the test results shown in Fig. 8, the roundness errors of the three circular paths in *xy*-, *yz*- and *xz*-plane were reduced from 27.3 μm, 20.7 μm and 24.1 μm to 9.2 μm, 12.3 μm and 7.8 μm, respectively, with error compensation. The roundness errors caused by geometric errors can be improved significantly, while the roundness errors caused by backlash, servo mismatch and machine vibration can hardly be compensated. The test results verify feasibility and effectivity of the proposed identification method with regularization algorithm.

6. Conclusions

A new measurement scheme is proposed for machine tools, and geometric error identification based on regularization method is explored to solve the ill-posed identification problem. According to the analysis, simulation and experiment results, the following conclusions can be drawn.

(1) An error model which can relate the DBB radius error directly to the machine tool geometric error components was established, and an efficient DBB measurement scheme was proposed, which can be performed with only one mounting of the DBB in order to avoid producing extra setup errors.

(2) Polynomial based error modeling was performed for the geometric error components of machine tools. Then the regularization method was applied for identification of the coefficients of the modeling functions, which can solve the ill-posed identification problem effectively.

(3) The identifiability of the error parameters was analyzed. All the error parameters in the proposed error model can be identified, except for three linear correlated ones, $\delta_{yx,1}$, $\delta_{zx,1}$ and $\delta_{zy,1}$. In addition, to make more geometric errors identifiable, the installation position of the DBB must meet two requirements: ball P_S is not in the spindle axis; and ball P_W is not in the longitudinal central axis of the worktable.

(4) Regularization method can be adopted in error identification of machine tool, and the results are stable and credible.

Acknowledgments

The work was supported by National Natural Science Foundation of China (grant numbers 51605324 and 51420105007) and EU H2020-MSCA-RISE Project (grant number 734272).

Nomenclature

$\boldsymbol{e}$	: Geometric error vector of DBB-machine system
$\boldsymbol{e}_i$	: Error vector composed of PDGEs and PIGEs of *i*-axis
$\boldsymbol{E}(i)$	: PDGEs of *i*-axis in twist form
$\boldsymbol{E}_i$	: PIGEs of *i*-axis in twist form
$\boldsymbol{H}_i$	: Mapping matrix at the *i*th measurement configuration
$\boldsymbol{I}_3$	: Unit matrix of order 3
l	: Nominal length of DBB
$\boldsymbol{n}$	: Nominal unit vector pointing from P_W to P_S
$\boldsymbol{p}$	: Parameter vector of geometric errors
$\hat{\boldsymbol{p}}$	: Identification result of $\boldsymbol{p}$
$\Delta\boldsymbol{r}_P$	: Volumetric error vector of point *P*
${}^j\boldsymbol{r}_i$	: Position vector of point *i* measured in frame *j*
$\hat{\boldsymbol{r}}$	: Skew-symmetric matrix of vector $\boldsymbol{r}$
$\Delta\boldsymbol{s}$	: Installation error of the magnetic center mount
tr(·)	: Trace of matrix
$\delta_j(i)$	: Translational error of *i*-axis in *j*-direction between frame *X'*-*xyz* and *X*-*xyz*
$\delta_{ij,k}$	: The *k*th coefficient of the polynomial model of $\delta_j(i)$
$\varepsilon_j(i)$	: Angular error of *i*-axis in *j*-direction between frame *X'*-*xyz* and *X*-*xyz*
$\varepsilon_{ij,k}$	: The *k*th coefficient of the polynomial model of $\varepsilon_j(i)$
ε_{ij}	: Squareness error between *i*-axis and *j*-axis
μ	: Regularization parameter
μ^*	: GCV solution of regularization parameter

References

[1] H. Schwenke et al., Geometric error measurement and compensation of machines - An update, *CIRP Annals - Manufacturing Technology*, 57 (2) (2008) 660-675.

[2] R. Ramesh, M. A. Mannan and A. N. Poo, Error compensation in machine tools—A review: Part I: Geometric, cutting-force induced and fixture-dependent errors, *International J. of*

Machine Tools and Manufacture, 40 (9) (2000) 1235-1256.

[3] H. Liu et al., Configuration design and accuracy analysis of a novel magnetorheological finishing machine tool for concave surfaces with small radius of curvature, *J. of Mechanical Science and Technology*, 30 (7) (2016) 3301-3311.

[4] W. Tian et al., A general approach for error modeling of machine tools, *International J. of Machine Tools and Manufacture*, 79 (4) (2014) 17-23.

[5] S. Zhu et al., Integrated geometric error modeling, identification and compensation of CNC machine tools, *International J. of Machine Tools and Manufacture*, 52 (1) (2012) 24-29.

[6] K. I. Lee and S. H. Yang, Measurement and verification of position-independent geometric errors of a five-axis machine tool using a double ball-bar, *International J. of Machine Tools and Manufacture*, 70 (4) (2013) 45-52.

[7] F. Bauer and M. A. Lukas, Comparing parameter choice methods for regularization of ill-posed problems, *Mathematics and Computers in Simulation*, 81 (9) (2011) 1795-1841.

[8] C. B. Lee and S. K. Lee, Multi-degree-of-freedom motion error measurement in an ultraprecision machine using laser encoder - Review, *J. of Mechanical Science and Technology*, 27 (1) (2013) 141-152.

[9] G. Zhong et al., Position geometric error modeling, identification and compensation for large 5-axis machining center prototype, *International J. of Machine Tools and Manufacture*, 89 (2015) 142-150.

[10] Z. Usop et al., Measuring of positioning, circularity and static errors of a CNC vertical machining centre for validating the machining accuracy, *Measurement*, 61 (2015) 39-50.

[11] M. Rahmani and F. Bleicher, Experimental and numerical studies of the influence of geometric deviations in the performance of machine tools linear guides, *Procedia CIRP*, 41 (2016) 818-823.

[12] S. R. Park, T. K. Hoang and S. H. Yang, A new optical measurement system for determining the geometrical errors of rotary axis of a 5-axis miniaturized machine tool, *J. of Mechanical Science and Technology*, 24 (1) (2010) 175-179.

[13] B. Bringmann and W. Knapp, Model-based 'Chase-the-Ball' calibration of a 5-axes machining center, *CIRP Annals - Manufacturing Technology*, 55 (1) (2006) 531-534.

[14] A. Gąska et al., Analysis of changes in coordinate measuring machines accuracy made by different nodes density in geometrical errors correction matrix, *Measurement*, 68 (2015) 155-163.

[15] B. Bringmann, A. Küng and W. Knapp, A measuring artefact for true 3D machine testing and calibration, *CIRP Annals - Manufacturing Technology*, 54 (1) (2005) 471-474.

[16] S. Ibaraki, C. Oyama and H. Otsubo, Construction of an error map of rotary axes on a five-axis machining center by static R-test, *International J. of Machine Tools & Manufacture*, 51 (3) (2011) 190-200.

[17] Z. Zhang and H. Hu, Three-point method for measuring the geometric error components of linear and rotary axes based on sequential multilateration, *J. of Mechanical Science and Technology*, 27 (9) (2013) 2801-2811.

[18] J. B. Bryan, A simple method for testing measuring machines and machine tools Part 1: Principles and applications, *Precision Engineering*, 4 (2) (1982) 61-69.

[19] J. B. Bryan, A simple method for testing measuring machines and machine tools. Part 2: Construction details, *Precision Engineering*, 4 (3) (1982) 125-138.

[20] X. Jiang and R. J. Cripps, A method of testing position independent geometric errors in rotary axes of a five-axis machine tool using a double ball bar, *International J. of Machine Tools and Manufacture*, 89 (2015) 151-158.

[21] K. I. Lee and S. H. Yang, Accuracy evaluation of machine tools by modeling spherical deviation based on double ball-bar measurements, *International J. of Machine Tools and Manufacture*, 75 (12) (2013) 46-54.

[22] Z. Jiang et al., Single setup identification of component errors for rotary axes on five-axis machine tools based on pre-layout of target points and shift of measuring reference, *International J. of Machine Tools and Manufacture*, 98 (4/5) (2015) 1-11.

[23] D. Chen et al., Prediction and identification of rotary axes error of non-orthogonal five-axis machine tool, *International J. of Machine Tools and Manufacture*, 94 (2015) 74-87.

[24] A. N. Tikhonov, On stability of inverse problems, *Doklady Akademii Nauk USSR*, 39 (5) (1943) 195-198.

[25] Y. Lin, L. Bao and Y. Cao, Augmented Arnoldi-Tikhonov regularization methods for solving large-scale linear ill-posed systems, *Mathematical Problems in Engineering*, 2013 (5) (2014) 87-118.

[26] C. Ma and H. Hua, Force identification technique by the homotopy method, *J. of Mechanical Science and Technology*, 29 (10) (2015) 4083-4091.

[27] F. Cheng and W. Ji, Simultaneous identification of bearing dynamic coefficients in a water-gas lubricated hydrostatic spindle with a big thrust disc, *J. of Mechanical Science and Technology*, 30 (9) (2016) 4095-4107.

[28] D. M. Lee et al., Identification and measurement of geometric errors for a five-axis machine tool with a tilting head using a double ball-bar, *International J. of Precision Engineering and Manufacturing*, 12 (2) (2011) 337-343.

[29] G. Chen et al., Volumetric error modeling and sensitivity analysis for designing a five-axis ultra-precision machine tool, *International J. of Advanced Manufacturing Technology*, 68 (9-12) (2013) 2525-2534.

[30] L. W. Tsai, *Robot analysis: The mechanics of serial and parallel manipulators*, New York: Wiley (1999).

[31] RENISHAW PLC, *Renishaw ballbar help, Ballbar 20 software,* Wottonunder-Edge, United Kingdom: Renishaw.

[32] A. E. Hoerl and R. W. Kennard, Ridge regression: Biased estimation for non-orthogonal problems, *Technometrics*, 12 (1) (1970) 55-67.

[33] G. H. Golub, M. Heath and G. Wahba, Generalized cross-validation as a method for choosing a good ridge parameter, *Technometrics*, 21 (1979) 215-223.

[34] G. Wahba, Practical approximate solutions to linear operator equations when the data are noisy, *Advances in Applied Probability*, 14 (1976) 651-667.

Wenjie Tian is a lecturer of the School of Marine Science and Technology, Tianjin University, China. He received his Dr. Eng. from Tianjin University in 2015. His research interests include error modeling, error compensation, accuracy design of machine tools and industrial robots.

Weiguo Gao is a Associate Professor of the Key Laboratory of Mechanism Theory and Equipment Design of Ministry of Education, Tianjin University, China. He received his Dr. Eng. from Tianjin University in 2007. His research interests include thermal characteristics analysis, thermal error compensation, and thermal balance design of precision machine tools.